

ChemComm

Chemical Communications

rsc.li/chemcomm



ISSN 1359-7345

COMMUNICATION

Dianming Sun, Xiao-Hong Zhang, Eli Zysman-Colman *et al.*
A fluorene-bridged double carbonyl/amine multiresonant
thermally activated delayed fluorescence emitter for
efficient green OLEDs



Cite this: *Chem. Commun.*, 2024, 60, 2489

Received 25th November 2023,
Accepted 21st December 2023

DOI: 10.1039/d3cc05761e

rsc.li/chemcomm

A fluorene-bridged double carbonyl/amine multiresonant thermally activated delayed fluorescence emitter for efficient green OLEDs†‡

Sen Wu,^{§a} Ya-Nan Hu,^{§b} Dianming Sun,^{*a} Kai Wang,^{ib} Xiao-Hong Zhang^{ib} *^{bc} and Eli Zysman-Colman^{id} *^a

Herein, we report a fluorene-bridged double carbonyl/amine-based MR TADF emitter DDiKta-F, formed by locking the conformation of the previously reported compound DDiKta. Using this strategy, DDiKta-F exhibited narrower, brighter, and red-shifted emission. The OLEDs with DDiKta-F emitted at 493 nm and showed an EQE_{max} of 15.3% with an efficiency roll-off of 35% at 100 cd m⁻².

Thermally activated delayed fluorescence (TADF) materials have demonstrated great potential as next-generation emitters in organic light-emitting diodes (OLEDs) due to their ability to harness 100% of the excitons to produce light without the need for noble metals, present in phosphorescent OLEDs. TADF compounds convert non-emission triplet excitons into emissive singlets by an endothermic upconversion reverse intersystem crossing (RISC) process.^{1–4} The efficiency of the RISC process is governed in part by the singlet-triplet energy gap, ΔE_{ST} .⁵ A strongly twisted structure that effectively reduces the conjugation between donor and acceptor moieties is one strategy to achieve a small ΔE_{ST} as the exchange integral of the frontier molecular orbitals (FMOs) is small.⁴ However, a twisted structure exhibits significant excited-state structural relaxation, resulting in a broad emission characterized by a full width at half maximum (FWHM) higher than 70 nm.⁶ To compensate for the

broad emission, filters or microcavities are required to improve color purity; however, this can, unfortunately, reduce the device efficiency.⁷

Multiresonant TADF (MR-TADF) emitters have emerged as a potential solution as these rigid structures exhibit narrowband emission. First reported by Hatakeyama *et al.*, these compounds are p- and n-doped polycyclic aromatic hydrocarbons (PAHs).⁸ By employing this approach, the singlet and triplet excited states possess an alternating pattern of increasing and decreasing electron density compared to the ground state, thus enabling a small exchange integral and consequently a small ΔE_{ST} .⁹ The rigid structure and the short-range charge transfer (SRCT) nature of the excited states endow the MR-TADF compounds with bright, narrowband emission. Since the first report of MR-TADF emitters used in OLEDs in 2016, there has been intense research focused on expanding the chemical space encompassed by this class of emitters.¹⁰ In the original works of Hatakeyama *et al.*, the n-dopants were boron atoms. It is possible to replace these with carbonyl groups, and the groups of Zysman-Colman¹¹ Zhang,¹² and Jiang and Liao¹³ were among the first to report examples of MR-TADF emitters containing this motif. Expanding the MR-TADF skeleton has been demonstrated to be an effective strategy for improving the performance of MR-TADF emitters,¹⁴ which has been less explored in carbonyl/amine systems.

We have shown that the dimerization of the MR-TADF emitter, DiKta, in DDiKta, leads to a modest red-shift of the emission and the OLED showed an improved performance.¹⁵ In an attempt to further improve the device performance and reduce the structural motion inherent in DDiKta, here, we envisioned annealing together two DiKta units through a central 9,9-dimethyl-9H-fluorene bridge, DDiKta-F. An analogue without the *tert*-butyl groups was also synthesized; however, purification proved too difficult owing to its poor solubility, likely due to its strong propensity to aggregate. Therefore, two *tert*-butyl groups were added to improve the solubility of this compound. DDiKta-F was found to be brighter (photoluminescence quantum yield, Φ_{PL} , of 78%) and emits with a narrower FWHM, of 49 nm compared to DDiKta (Φ_{PL} of 68% and FWHM of 59 nm) in 2 wt% doped films in 1,

^a Organic Semiconductor Centre, EaStCHEM School of Chemistry, University of St Andrews, St Andrews, Fife KY16 9ST, UK.
E-mail: eli.zysman-colman@st-andrews.ac.uk, sd235@st-andrews.ac.uk;
Fax: +44-1334 463808; Tel: +44-1334 463826

^b Institute of Functional Nano & Soft Materials (FUNSOM), Joint International Research Laboratory of Carbon-Based Functional Materials and Devices, Soochow University, Suzhou, Jiangsu 215123, P. R. China.
E-mail: xiaohong_zhang@suda.edu.cn

^c Jiangsu Key Laboratory of Advanced Negative Carbon Technologies, Soochow University, Suzhou, Jiangsu, 215123, P. R. China

† Electronic supplementary information (ESI) available: ¹H and ¹³C-NMR spectra, HRMS, EA and HPLC of all target compounds; supplementary computational, photophysical device data. See DOI: <https://doi.org/10.1039/d3cc05761e>

‡ The research data supporting this publication can be accessed at <https://doi.org/10.17630/87972673-41de-4d34-9fd1-cfd23e633741>

§ Equal contribution.



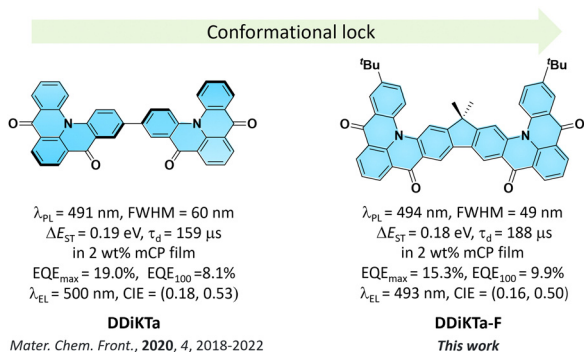


Fig. 1 Chemical structures, photophysical properties and device properties of **DDiKta** and **DDiKta-F**.

3-bis(carbazolyl)benzene (mCP). The device with **DDiKta-F** showed an EQE_{max} of 15.3% emitting at a λ_{EL} of 493 nm (FWHM of 46 nm) with an improved efficiency roll-off at 100 cd m^{-2} of 35% compared to the devices with **DDiKta** (56%)¹⁵ and **DikTa** (44%) (Fig. 1).¹¹

Theoretical calculations were out to investigate the effect of the incorporation of the fluorene bridge on the optoelectrical properties of the emitter compared to those of the reference, **DikTa**. The geometry in the ground state was first optimized using density functional theory at the PBE0/6-31G(d,p) level. The frontier molecular orbitals (FMOs) are delocalized over the entire π -conjugated system, and the HOMO and LUMO show an alternating distribution pattern similar to that of **DDiKta**, which is emblematic of MR-TADF compounds.¹⁵ The calculated HOMO and LUMO levels of **DDiKta-F** are -5.94 and -2.32 eV, respectively. The HOMO–LUMO gap of 3.62 eV for **DDiKta-F** is smaller than that of **DDiKta** ($\Delta E_{\text{HOMO-LUMO}} = 3.70$ eV), reflecting an increased conjugation in the former. The locked structure of the molecule contributed to small geometric changes between the S_0 and S_1 states, as depicted in Fig. S15 (ESI†). Thus, it is expected that the emission spectrum will be narrow and that there will be a small Stokes shift. The emission spectra of both **DikTa** and **DDiKta-F** under vacuum were simulated using Frank–Condon analysis based on the S_1 – S_0 transition at the TDA-DFT-PBE0/6-31G(d,p) level (Fig. S16, ESI†). The simulated spectrum of **DikTa** shows an emission band peaking at $\lambda_{\text{PL}} = 428$ nm and a small FWHM = 14 nm, which closely aligns with the emission in hexane at $\lambda_{\text{PL}} = 436$ nm (FWHM = 21 nm). By contrast, the simulated emission spectrum of **DDiKta-F** is red-shifted at $\lambda_{\text{PL}} = 474$ nm and is slightly broader (FWHM = 18 nm). We previously demonstrated that DFT calculations do not accurately predict the excited-state properties of MR-TADF emitters.¹⁶ Here, we employed SCS-ADC(2)/cc-pVDZ calculations to accurately model the excited states of **DDiKta-F**.¹⁶ Difference density plots provide information on the changes in the electron density distribution in the excited states compared to that of the ground state. The difference density plots between S_0 and each of the S_1 and T_1 states, calculated for the S_0 optimized geometry, reveal that these excited states have SRCT characteristics typical of MR-TADF emitters. The calculated energies of the S_1 and T_1 states are 3.34 and 3.08 eV, respectively, which are lower than those of **DikTa** ($S_1/T_1 = 3.45/3.18$ eV) and **DDiKta** ($S_1/T_1 = 3.39/3.12$ eV), indicating that the emission in this compound should be red-shifted compared



Fig. 2 (a) Distribution of FMOs of **DDiKta-F**, calculated at the PBE0/6-31G(d,p) level. (b) Difference density plots of S_1/S_2 and T_1/T_2 excited states, calculated at the SCS-ADC(2)/cc-pVDZ level for **DDiKta-F**, where f is the oscillator strength. The dashed lines in each figure reference the calculated values of **DikTa** at the same level of theory.¹⁷

to the two reference emitters. The calculated ΔE_{ST} for **DDiKta-F** is 0.26 eV, which is similar to those of **DikTa** (0.26 eV)¹⁷ and **DDiKta** (0.27 eV) (Fig. 2).¹⁵

The calculated spin–orbit coupling matrix element (SOCME) value between S_1 and T_1 is 0.37 cm^{-1} based on the T_1 -optimized geometry, while the SOCME values between S_1 and the four closely lying higher triplet excited states range from 0.07 to 5.93 cm^{-1} . In particular, the large $\langle S_1 | \hat{H}_{\text{SOC}} | T_3 \rangle$ value of 5.93 cm^{-1} is attributed to an n – π^* transition localized on the carbonyl groups (Fig. S18, ESI†).¹⁷ These closely lying intermediate triplet states can participate in the RISC mechanism between T_1 and S_1 mediated by spin-vibronic coupling.¹⁸

The electrochemical properties of **DDiKta-F** and **DikTa** were investigated using cyclic voltammetry (CV) and differential pulse voltammetry (DPV) in deaerated DCM with 0.1 M tetra- n -butylammonium hexafluorophosphate as the supporting electrolyte (Fig. S19, ESI†). The CV results show that the oxidation is irreversible while the reduction is a quasi-reversible process. The oxidation and reduction potentials, E_{ox} and E_{red} , determined, respectively, from the first oxidation and reduction peaks of the DPV, are 1.34 and -1.48 V vs. SCE. The corresponding HOMO/LUMO levels and energy gap (ΔE) are $-5.68/-2.86$ and 2.82 eV, respectively. The HOMO/LUMO are both destabilized compared to those of **DDiKta** ($-5.97/-3.07$ eV)¹⁵ and **DikTa** ($-6.10/-2.99$ eV), implying that the fluorene bridge acts as an electron donor. As a result, ΔE was smaller than those of **DDiKta** (2.90 eV) and **DikTa** (3.03 eV).

The absorption spectrum of the diluted toluene solution (10^{-5} M), shown in Fig. 3, exhibits two major bands. The band between 300 and 400 nm is linked to a π – π^* transition delocalized over the whole skeleton, and the band at 375 nm is associated with the absorption of the central fluorene unit, both assigned from analysis of the TDA-DFT calculations (Fig. S17, ESI†). The lower energy band at 453 nm and shoulder at 431 nm are characteristics of an SRCT excited state transition for MR-TADF emitters (Fig. S17, ESI†). The SRCT band of **DDiKta-F** is red-shifted and more intense ($\epsilon = 25 \times 10^3 \text{ M}^{-1} \text{ cm}^{-1}$) than those of **DDiKta** ($\lambda_{\text{abs}} = 440$ nm and $\epsilon = 10.4 \times 10^3 \text{ M}^{-1} \text{ cm}^{-1}$) and **DikTa** ($\lambda_{\text{abs}} = 433$ nm and $\epsilon = 21 \times 10^3 \text{ M}^{-1} \text{ cm}^{-1}$) due in part to its larger π -conjugation.¹⁵ The photoluminescence (PL) spectrum of **DDiKta-F** in toluene, shown in



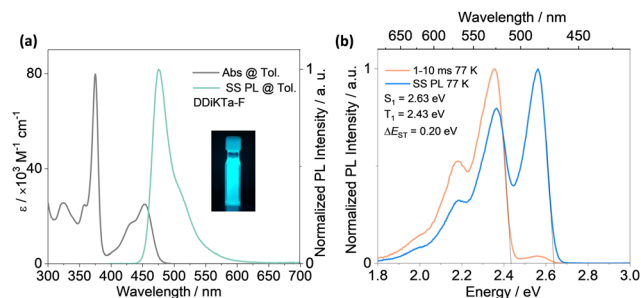


Fig. 3 (a) Absorption and SS PL spectra obtained in toluene at RT. Inset: Photograph of **DDiKta-F** in toluene and irradiated with a UV torch ($\lambda_{\text{exc}} = 365$ nm). (b) SS PL and delayed emission spectra (1–10 ms), collected in 2-MeTHF at 77 K ($\lambda_{\text{exc}} = 340$ nm).

Fig. 3a, has a peak maximum, λ_{PL} , of 476 nm, a shoulder at 511 nm, and an FWHM of 32 nm. The shoulder peak arises from the vibrational energy levels of the molecule, a typical characteristic of MR-TADF emitters.^{19,20} This emission is red-shifted compared to those of **DDiKta** ($\lambda_{\text{PL}} = 470$ nm) and **DiKta** ($\lambda_{\text{PL}} = 453$ nm).¹⁵ The emission of **DDiKta-F** shows a modest positive solvatochromism (Fig. S20, ESI†), which is consistent with the emissive excited state of SRCT. The energies of the S_1 and T_1 states, determined from the onsets of the steady-state PL and phosphorescence spectra at 77 K in 2-MeTHF glass are 2.63 and 2.43 eV, respectively (Fig. 3b); thus, $\Delta E_{\text{ST}} = 0.20$ eV. This value is similar in magnitude to those of **DiKta** (0.22 eV in frozen toluene) and **DDiKta** (0.21 eV in frozen toluene). The photoluminescence quantum yield, Φ_{PL} , in toluene is 34%, which decreases to 31% upon exposure to air (Fig. S21, ESI†). No delayed emission was observed in toluene and the lifetime of the emission decay, τ_{PL} , was 4.5 ns (Fig. S21, ESI†), which is similar to that of **DiKta** ($\tau_{\text{PL}} = 5.1$ ns).¹¹

With a view to employ **DDiKta-F** as an emitter in OLEDs and to cross-compare their device performance with those of **DDiKta** and **DiKta**, we next investigated the photophysical properties of this emitter as doped films in mCP. The 2 wt% doped film of **DDiKta-F** in mCP emits at 494 nm with a FWHM of 49 nm (Fig. 4a), an emission that is red-shifted compared to those of **DDiKta** ($\lambda_{\text{PL}} = 491$ nm) and **DiKta** ($\lambda_{\text{PL}} = 467$ nm) in 2 wt% doped films in mCP.¹⁷ We identified that 2 wt% doping provided the highest Φ_{PL} of 78%, while the Φ_{PL} decreased to 43% and the PL spectrum showed a pronounced red-shift from 491 to 507 nm when the doping concentration increased from 1 wt% to 10 wt% (Fig. S22, ESI†), implying that aggregation becomes an issue at this higher doping concentration. The Φ_{PL} of the 2 wt% doped film in mCP decreased to 65% in air. The Φ_{PL} of **DDiKta-F** is slightly higher than those of both **DiKta** ($\Phi_{\text{PL}} = 46\%$) and **DDiKta** ($\Phi_{\text{PL}} = 65\%$) in 2 wt% doped films in mCP. At the same doping concentration, the Φ_{PL} in the phosphine oxide-based hosts DPEPO and PPT are similar at 74 and 61% but the λ_{PL} are red-shifted at 510 and 511 nm, respectively, due to their higher polarity (Fig. S23, ESI†). The S_1/T_1 energies, determined from the onsets of the steady-state PL and delayed emission spectra at 77 K in the 2 wt% doped films in mCP, are 2.58/2.40 eV, resulting in a ΔE_{ST} of 0.18 eV (Fig. S26, ESI†), which



Fig. 4 (a) SS PL spectra ($\lambda_{\text{exc}} = 340$ nm); (b) time-resolved PL decays of **DDiKta** and **DDiKta-F** measured using MCS (inset: TRPL decays of the prompt component measured using TCSPC); $\lambda_{\text{exc}} = 375$ nm.

is similar to that measured for 2-MeTHF glass. Temperature-dependent transient PL decay analysis reveals the expected increase in the delayed emission with increasing temperature, which confirms the TADF in the 2 wt% doped film in mCP (Fig. S24, ESI†). The emission decays with the associated average prompt (τ_{p}) and delayed (τ_{d}) lifetimes are 5.6 ns and 188 μs (Table 1), respectively. These values are intermediate to those of **DDiKta** ($\tau_{\text{p}} = 5.9$ ns and $\tau_{\text{d}} = 159$ μs) and **DiKta** ($\tau_{\text{p}} = 4.8$ ns and $\tau_{\text{d}} = 242$ μs); in air, the delayed emission of **DDiKta-F** was not completely quenched (Fig. S25, ESI†). From these photophysical measurements, the RISC rate constant (k_{RISC}) of **DDiKta-F** was determined to be $2.16 \times 10^4 \text{ s}^{-1}$ (Table S2, ESI†),^{21,22} which is intermediate to those of **DDiKta** ($k_{\text{RISC}} = 1.77 \times 10^4 \text{ s}^{-1}$) and **DiKta** ($k_{\text{RISC}} = 2.52 \times 10^4 \text{ s}^{-1}$).

Having identified the potential of **DDiKta-F** as an emitter for OLEDs, we next fabricated vacuum-deposited devices. The devices have the following architecture: ITO/TAPC (35 nm)/TCTA (10 nm)/CzSi (10 nm)/x wt% emitter/mCP (20 nm)/TmPyPB (40 nm)/LiF (1 nm)/Al (100 nm), where indium tin oxide (ITO) is the anode and 4,4'-cyclohexylidenebis[N,N-bis(4-methylphenyl)benzenamine] (TAPC) acts as the hole-transport layer. 9-(4-*tert*-butylphenyl)-3,6-bis(triphenylsilyl)-9H-carbazole (CzSi) is the exciton blocking layer, 1,3,5-tri(*m*-pyridin-3-ylphenyl)benzene (TmPyPB) acts as the electron-transporting material, and LiF modifies the work function of the aluminium cathode. The chemical structures of the materials used in these devices are shown in Fig. S27 (ESI†). The device stacks and their related performance are shown in Fig. 5 and Fig. S28 and S29 (ESI†), respectively.

The electroluminescence peak of the OLED, λ_{EL} of 493 nm and FWHM of 46 nm match those of the PL spectrum of the 2 wt% films in mCP ($\lambda_{\text{PL}} = 494$ nm and FWHM = 49 nm). The EL is narrower compared to the previously reported device with

Table 1 Photophysical data of **DDiKta-F** and **DDiKta** in 2 wt% doped films in mCP

Emitter	Φ_{PL}^a / %	$\lambda_{\text{PL}}/\text{nm}$	FWHM/nm	S_1^b/T_1^c / eV	$\Delta E_{\text{ST}}/\text{eV}$	$\tau_{\text{p}}, \tau_{\text{d}}/\text{ns}, \mu\text{s}$
DDiKta-F	78	494	49	2.58, 2.40	0.18	5.6, 188
DDiKta	68	491	60	2.64, 2.45	0.19	5.9, 159
DiKta ¹⁷	46	467	46	2.75, 2.55	0.20 ¹¹	4.8, 242

^a Φ_{PL} was measured using an integrating sphere under nitrogen ($\lambda_{\text{exc}} = 340$ nm). ^b Obtained from the onset of the SS PL spectrum at 77 K. ^c Obtained from the onset of the delayed emission spectrum (1–10 ms) at 77 K ($\lambda_{\text{exc}} = 340$ nm).



Fig. 5 (a) Device configuration and energy levels for each layer; (b) electroluminescence spectra for devices; (c) J - V - L characteristics; and (d) EQE and CE versus luminance characteristics.

DDiKta (9 wt% in DPEPO), which emitted at a λ_{EL} of 500 nm and had an FWHM of 59 nm.¹⁵ This small red-shifted emission compared to the SS PL in 2 wt% mCP film can be attributed to a combination of the use of the higher polarity DPEPO host and higher doping concentrations. By contrast, the EL is red-shifted compared to the device with **DiKta** (3.5 wt% in mCP), which emitted at a λ_{EL} of 465 nm and had a FWHM of 59 nm.¹¹ The corresponding Commission Internationale de l'Éclairage (CIE) coordinates are (0.16, 0.50) for the device with **DDiKta-F**, which are close to those of the device with **DDiKta** (0.18, 0.53), yet are red-shifted compared to the device with **DiKta** (0.14, 0.18). The device with **DDiKta-F** exhibited an EQE_{max} of 15.3%, which is similar to those of **DDiKta** (19.0%) and **DiKta** (14.7%). Gratifyingly, the efficiency roll-off was less severe, with an EQE of 100 cd m⁻² at 9.9% for the device with **DDiKta-F**, which was higher than those of **DDiKta** (EQE_{100} = 8.1%) and **DiKta** (EQE_{100} = 8.3%). This modestly improved efficiency roll-off can be explained by a higher figure of merit (FOM) that describes productive exciton utilization, $FOM = \frac{k_r k_{RISC}}{k_{ISC}}$,²³ of 4.75×10^3 s⁻¹ for **DDiKta-F**, compared to those of 4.71×10^3 and 1.87×10^3 s⁻¹ for **DDiKta** and **DiKta**, respectively.

In conclusion, we demonstrated an easy-to-access synthetic route for constructing a p-extended dimeric MR-TADF emitter by fusing two **DiKta** units onto a fluorene bridge. Through this strategy, the structural motion was reduced compared to that of the parent dimeric emitter **DDiKta**. This led to an improved Φ_{PL} of 79% and a red-shifted and narrower emission at 494 nm (FWHM = 49 nm) in 2 wt% doped films in mCP. Moreover, the ΔE_{ST} decreased to 0.18 eV, which led to a modest improvement in k_{RISC} from 1.77×10^4 s⁻¹ to 2.16×10^4 s⁻¹. The device with **DDiKta-F** exhibited an EQE_{max} of 15.3% and emission at 493 nm. Owing to the faster k_{RISC} , the device exhibited a smaller efficiency roll-off of 35% at 100 cd m⁻² than the devices with **DDiKta** (56%) and **DiKta** (44%). This emitter design, annelating multiple MR-TADF cores about a central fluorene, provides

a simple method to maintain narrowband emission in MR-TADF compounds while simultaneously enhancing the Φ_{PL} and k_{RISC} .

S. W. thanks the China Scholarship Council (201906250199) for support. D.S. acknowledges support from the Royal Academy of Engineering Enterprise Fellowship (EF2122-13106). E. Z.-C. thanks the Engineering and Physical Sciences Research Council (EP/W015137/1, EP/W007517) for support. X.-H. Z. acknowledges support from the National Natural Science Foundation of China (Grant No. 52130304, 51821002) and the Collaborative Innovation Center of Suzhou Nano Science & Technology.

Conflicts of interest

There are no conflicts to declare.

References

- 1 C. W. Tang and S. A. VanSlyke, *Appl. Phys. Lett.*, 1987, **51**, 913.
- 2 M. A. Baldo, D. F. O'Brien, Y. You, A. Shoustikov, S. Sibley, M. E. Thompson and S. R. Forrest, *Nature*, 1998, **395**, 151–154.
- 3 A. Endo, K. Sato, K. Yoshimura, T. Kai, A. Kawada, H. Miyazaki and C. Adachi, *Appl. Phys. Lett.*, 2011, **98**, 083302.
- 4 Y. Tao, K. Yuan, T. Chen, P. Xu, H. Li, R. Chen, C. Zheng, L. Zhang and W. Huang, *Adv. Mater.*, 2014, **26**, 7931–7958.
- 5 H. Uoyama, K. Goushi, K. Shizu, H. Nomura and C. Adachi, *Nature*, 2012, **492**, 234–238.
- 6 Y. J. Cho, S. K. Jeon, S.-S. Lee, E. Yu and J. Y. Lee, *Chem. Mater.*, 2016, **28**, 5400–5405.
- 7 A. C. Arsenault, D. P. Puzzo, I. Manners and G. A. Ozin, *Nat. Photonics*, 2007, **1**, 468–472.
- 8 T. Hatakeyama, K. Shiren, K. Nakajima, S. Nomura, S. Nakatsuka, K. Kinoshita, J. Ni, Y. Ono and T. Ikuta, *Adv. Mater.*, 2016, **28**, 2777–2781.
- 9 H. Jiang, J. Jin and W. Y. Wong, *Adv. Funct. Mater.*, 2023, **33**, 2306880.
- 10 R. K. Konidena and K. R. Naveen, *Adv. Photonics Res.*, 2022, **3**, 2200201.
- 11 D. Hall, S. M. Suresh, P. L. dos Santos, E. Duda, S. Bagnich, A. Pershin, P. Rajamalli, D. B. Cordes, A. M. Z. Slawin, D. Beljonne, A. Köhler, I. D. W. Samuel, Y. Olivier and E. Zysman-Colman, *Adv. Opt. Mater.*, 2020, **8**, 1901627.
- 12 X. Li, Y.-Z. Shi, K. Wang, M. Zhang, C.-J. Zheng, D.-M. Sun, G.-L. Dai, X.-C. Fan, D.-Q. Wang, W. Liu, Y.-Q. Li, J. Yu, X.-M. Ou, C. Adachi and X.-H. Zhang, *ACS Appl. Mater. Interfaces*, 2019, **11**, 13472–13480.
- 13 Y. Yuan, X. Tang, X.-Y. Du, Y. Hu, Y.-J. Yu, Z.-Q. Jiang, L.-S. Liao and S.-T. Lee, *Adv. Opt. Mater.*, 2019, **7**, 1801536.
- 14 C. Zhou, A. Shatskiy, A. Z. Temerdashev, M. D. Kärkäs and P. Dinér, *Commun. Chem.*, 2022, **5**, 92.
- 15 D. Sun, S. M. Suresh, D. Hall, M. Zhang, C. Si, D. B. Cordes, A. M. Z. Slawin, Y. Olivier, X. Zhang and E. Zysman-Colman, *Mater. Chem. Front.*, 2020, **4**, 2018–2022.
- 16 D. Hall, J. C. Sancho-García, A. Pershin, G. Ricci, D. Beljonne, E. Zysman-Colman and Y. Olivier, *J. Chem. Theory Comput.*, 2022, **18**, 4903–4918.
- 17 S. Wu, L. Zhang, J. Wang, A. Kumar Gupta, I. D. W. Samuel and E. Zysman-Colman, *Angew. Chem., Int. Ed.*, 2023, **62**, e202305182.
- 18 T. J. Penfold, E. Gindensperger, C. Daniel and C. M. Marian, *Chem. Rev.*, 2018, **118**, 6975–7025.
- 19 Y. Kondo, K. Yoshiura, S. Kitera, H. Nishi, S. Oda, H. Gotoh, Y. Sasada, M. Yanai and T. Hatakeyama, *Nat. Photon.*, 2019, **13**, 678.
- 20 X. Qiu, G. Tian, C. Lin, Y. Pan, X. Ye, B. Wang, D. Ma, D. Hu, Y. Luo and Y. Ma, *Adv. Opt. Mater.*, 2020, **9**, 20200.
- 21 K. Masui, H. Nakanotani and C. Adachi, *Org. Electron.*, 2013, **14**, 2721–2726.
- 22 Y. Tsuchiya, S. Diesing, F. Bencheikh, Y. Wada, P. L. dos Santos, H. Kaji, E. Zysman-Colman, I. D. W. Samuel and C. Adachi, *J. Phys. Chem. A*, 2021, **125**, 8074–8089.
- 23 S. Diesing, L. Zhang, E. Zysman-Colman and I. Samuel, *ChemRxiv*, 2023, preprint, DOI: [10.26434/chemrxiv-2023-c0hgg](https://doi.org/10.26434/chemrxiv-2023-c0hgg).

